NJC

PAPER

View Article Online
View Journal | View Issue

Check for updates

Cite this: *New J. Chem.*, 2024, **48**, 7863

Regulating the particle sizes of NaA molecular sieves toward enhanced heavy metal ion adsorption†

WenLi Cui,‡[a] Ke Tang,‡[a] Yunqiang Chen,[b] Zhou Chen,[a] Yihong Lan,[b] YuBin Hong*[b] and WeiGuang Lan*[ab]

Heavy metal ions have a serious effect on humans and the ecosystem. Molecular sieves have attracted significant attention in heavy metal ion adsorption with distinct microporosity and uniform pore size. In this paper, we successfully synthesized nano-sized NaA molecular sieves in the presence of an organic templating agent while aluminum isopropoxide and silica sol were used as the aluminum and silica sources. To synthesize molecular sieves of the ideal size, the anionic cation concentration and templating agent were adjusted. The findings of Cu(II) and Pb(II) adsorption on NaA molecular sieves showed that under the ideal conditions of adsorption time at 90 minutes, pH = 5, adsorption temperature at 25 °C, and starting adsorbent concentration at 100 mg g^{-1}, the optimal adsorbing capacity could reach 230 mg g^{-1} and 600 mg g^{-1}, respectively. Isotherm, kinetic, thermodynamic and reusability studies of heavy metal ion adsorption on NaA molecular sieves were carried out to investigate the adsorption kinetics. This work provides a new avenue to regulate the particle sizes of molecular sieves to enhance the adsorption capacity of heavy metal ions.

Received 25th December 2023,
Accepted 25th March 2024

DOI: 10.1039/d3nj05924c

rsc.li/njc

1. Introduction

Heavy metal ions, which are widely employed as crucial raw materials in industrial production, including printing, electroplating, metallurgy, textiles, metal processing, ceramics, and many other industries, pose a serious threat to the environment and human health. Because heavy metal ions cannot be broken down by organisms, they persist for a long time in the human body. High levels of copper in the body can cause headaches, vomiting, nausea, liver and kidney failure, respiratory problems and abdominal pain.[1] Furthermore, lead damages the kidneys, liver, reproductive system and brain function.[2] A buildup of heavy metal ions can harm the body and its internal organs,[3,4] and it can even result in cancer.[5] Therefore, it is essential to explore ways to treat heavy metal ion pollutants in wastewater.

Various processes have been used to remove heavy metal ions, including membrane separation, coagulation, ultrafiltration, nanofiltration, adsorption, chemical precipitation, and solvent extraction.[6–11] These systems, however, have drawbacks such as high costs, high energy consumption, and poor metal ion removal in certain situations.[6] Adsorption is one of the most promising strategies for removing heavy metal ions,[12,13] with considerable advantages in terms of cost, environmental protection, and procedure. The most common adsorbents are molecular sieves, activated carbon, chitosan, hydrogels, and various biosorbents.[14–18] Niu *et al.* improved the adsorption capacity and adsorption selectivity of activated carbon for heavy metals by introducing dithiocarbamate functional groups. The maximum adsorption of Pb(II), Cd(II) and Cu(II) by DTC–AC was 203.36 mg g^{-1}, 102.89 mg g^{-1} and 53.13 mg g^{-1}, respectively.[3] Jin *et al.* synthesized l-cysteine functionalized magnetic hollow $MnFe_2O_4$ nanorods (H-$MnFe_2O_4$-Cys) for the purpose of removing heavy metal ions, specifically Cr^{6+} and Pb^{2+} from aqueous solutions. The adsorption capacities of H-$MnFe_2O_4$-Cys for Cr^{6+} and Pb^{2+} were determined to be 268.86 mg g^{-1} and 291.07 mg g^{-1}, respectively. These findings suggest that H-$MnFe_2O_4$-Cys nanorods exhibit significant potential for the efficient removal of heavy metal ions from contaminated water sources.[4]

Compared to these adsorbents, the advantages of molecular sieves in terms of low cost, high cation exchange capacity, non-emission of toxic compounds, and high selectivity have attracted much attention in the fields of heavy metal ions adsorption. Molecular sieves are crystalline microporous materials composed of aluminum silicate, and are categorized as either natural or

---

[a] *Xiamen University Center for Membrane Application and Advancement, College of Materials, Xiamen University, Xiamen 361005, Fujian, China. E-mail: wglan@xmu.edu.cn*

[b] *Suntar Membrane Technology (Xiamen) Co., Ltd., Xiamen 361022, Fujian, China. E-mail: hongyb@suntar.com*

† Electronic supplementary information (ESI) available. See DOI: **https://doi.org/10.1039/d3nj05924c**

‡ These authors contributed equally to this work.

synthetic. Synthetic molecular sieves exhibit higher purity, smaller particle sizes, and superior adsorption capabilities compared to their natural counterparts. Because of their distinctive microporosity and consistent pore size, molecular sieves are preferred for practical adsorption applications (SSZ-13). As a result, researchers have conducted extensive research on the synthesis of molecular sieves. Li *et al.* used fly ash from a power plant in Inner Mongolia as a raw material and desiliconization with sodium hydroxide as a silicon source. Utilizing P123 as the template, SBA-15 mesoporous molecular sieves were prepared, through a hydrothermal method. The adsorption equilibrium was reached within 60 min at 30 °C, pH = 5, and an initial concentration of Pb^{2+} of 100 mg L^{-1}. The removal of Pb^{2+} reached 97.22%, with 131 mg g^{-1} of saturation adsorption capacity.[19] Liang *et al.* synthesized zeolite NaX from coal gangue, a byproduct of coal extraction, and studied its ability to remove Cd^{2+} and Cu^{2+}. The highest adsorption of Cd^{2+} and Cu^{2+} by zeolite NaX was 100.11 mg g^{-1} and 95.29 mg g^{-1}, respectively.[20] Wang *et al.* produced CS–ZIF-8 molecular sieves by synthesizing ZIF-8 *in situ* using acid solubilization/alkali immobilization with chitosan as a carrier. The theoretical maximum adsorption of Cu(II) and Pb(II) by CS–ZIF-8 was 165.7 mg g^{-1} and 131.4 mg g^{-1}, respectively, with an optimal adsorption pH of 5, and the equilibrium time of adsorption of Cu(II) was 5 h and the equilibrium time for adsorption of Pb(II) was 2 h.[21] Currently, most molecular sieves are in the micrometer size range, which results in a lower saturated adsorption capacity and poor adsorption efficiency. The size of the molecular sieve has a great influence on its adsorption performance,[22–24] the adsorption performance tends to be limited by their relatively small specific surface area, less exposed crystalline cells, and longer transport paths; the smaller the particle size of the molecular sieve, the greater the pressure drop, while the larger the particle size, the lower the efficiency. Therefore, it is highly urgent to develop synthetic methods for nanoscale molecular sieves in order to improve adsorption efficiency.

In this study, nanoscale NaA molecular sieves were produced using a hydrothermal technique with tetramethylammonium hydroxide. By changing the exact synthesis settings, NaA-type molecular sieves with homogeneous forms and sizes 10 times smaller than those of industrial molecular sieves were produced. The properties of the products were investigated using a variety of techniques, including X-ray diffraction (XRD), field emission scanning electron microscopy (SEM), X-ray photoelectron spectroscopy (XPS), and energy spectrum analysis. The adsorption performance of molecular sieves on Cu(II) and Pb(II) was investigated, the reusability of NaA molecular sieves explored and the appropriate adsorption conditions and mechanism were optimized, providing the theoretical framework and technological support for the research of heavy metal ion removal from wastewater using molecular sieves.

2. Materials and methods

2.1. Materials and chemicals

Aluminum isopropoxide ($C_9H_{21}AlO_3$), silicone sols (SiO_2), nitric acid (HNO_3), and tetramethylammonium hydroxide ($C_4H_{13}NO$) were purchased from Shanghai McLean Company. Copper nitrate ($Cu(NO_3)_2$), lead nitrate ($Pb(NO_3)_2$), ethylenediaminetetraacetic acid (EDTA) and sodium hydroxide (NaOH) were purchased from Ciron Scientific.

2.2. Synthesis of nano-sized NaA molecular sieves

In this study, NaA molecular sieves were synthesized through the hydrothermal method using silica sol as the silicon source, aluminum isopropoxide as the aluminum source, sodium hydroxide to adjust the pH of the reaction system, and tetramethylammonium hydroxide as a template agent, and the molar ratio of the reaction system was $1Al_2O_3:2SiO_2:xNa_2O:y(TMA)_2O:350H_2O$. x represents the Na_2O molar ratio, and y represents the $(TMA)_2O$ molar ratio. x = 0.15, 0.3, 0.45, 0.6, and 0.75 were labelled A1, A2, A3, A4, and A5, respectively. The y-values for A1 to A5 were all 6, and x were all 0.3. y = 4, 8, and 10 were labelled A6, A7, and A8, respectively. The detail synthesis parameters are listed in Table S1 (ESI†).

In order to fabricate NaA molecular sieves, a certain amount of sodium hydroxide was dissolved in deionized water. Then a quantity of tetramethylammonium hydroxide was added, and the solution was divided into two equal parts of equal volume. Subsequently, the aluminate solution was prepared by dissolving aluminum isopropoxide in one of the solutions, while the silica solution was prepared by adding silica sol to the other one. After both solutions were completely dissolved, the silicate solution was poured into the aluminate solution, stirred well and put into the reactor for hydrothermal heating. Finally, the NaA molecular sieves were obtained by repeated centrifugation, dispersion, washing the sample with deionized water, and then drying in an oven.

2.3. Heavy metal ion adsorption and desorption experiment

A particular amount of molecular sieve was added to a 50 mL conical flask containing a solution of metal ions, and stirred until the adsorption reaction was completed. Adsorption experiments were performed at 25 °C, pH = 5. Centrifugation was performed after the adsorption was completed and the supernatant was sampled for testing. The concentration of the retained metal ions was detected by the AA-1800 atomic absorption spectrometer to evaluate the adsorption performance of the NaA molecular sieve for the adsorption of heavy metal ions. The adsorption capacity for heavy metal ions on the NaA molecular sieve was determined using eqn (1).[25–27]

$$q = \frac{(C_0 - C_e)V}{m} \tag{1}$$

where, q, C_0, C_e, m and V represent the adsorption capacity of the NaA molecular sieve (mg g^{-1}), initial heavy metal ion concentration (mg L^{-1}), heavy metal ion concentration after adsorption (mg L^{-1}), mass of NaA molecular sieve (g), and the volume of the adsorbed solution (L), respectively.

As for the desorption experiment, 10 mmol L^{-1} EDTA was used as the desorbent in this paper, and the molecular sieves adsorbed with heavy metal ions were put into the EDTA solution and stirred for 6 hours at 25 °C. After that, it was washed three times with deionized water, centrifuged and dried for preparation.

2.4. Characterization methods

X-ray diffraction (XRD, Bruker-axs, Germany) with a monochromatic Cu-Kα X-ray source was utilized to analyze the structure and crystallinity of NaA molecular sieves synthesized under different conditions. *In situ* FT-IR Spectrometer (FTIR, Bruker Vertex 70V) and XRD were utilized to study the NaA molecular sieves before and after the reaction. Microstructural characterization of NaA molecular sieves synthesized under different conditions was carried out using field emission scanning electron microscopy (FE-SEM, Hitachi SU-70, Japan). The elemental composition of NaA molecular sieves was analyzed by using energy dispersive X-ray spectroscopy (EDX). X-ray photoelectron spectroscopy (XPS, Thermo Scientific ESCALAB Xi+, USA) was used to study the elemental composition of the NaA molecular sieves before and after adsorption. Al-Kα radiation was used as the X-ray source, and the binding energies were referenced to the C 1s peak (284.8 eV). Absorption spectral characterization was carried out on a Mayan Analytical AA-1800 Atomic Absorption Spectrometer (AA-1800). Determination was carried out using the flame method at 283.31 nm and 324.75 nm, respectively.

3. Results and discussion

3.1. Synthesis of nano-sized NaA molecular sieves

3.1.1. XRD and crystallinity analysis. NaA molecular sieves are usually synthesized in the presence of a templating agent using alkali metal compounds to provide inorganic cations. Therefore, the concentration of inorganic cations is an important factor in the synthesis of NaA molecular sieves. On the one hand, the appropriate amount of inorganic cations is needed to promote the formation of molecular sieves, but inorganic cations with too low concentration can produce heterogeneous sieves compared to *e.g.* FAU-type molecular sieves.[28,29] On the other hand, basic cations with too high concentration lead to flocculation of the gel particles due to the accelerated dissolution rate, which is detrimental to the crystallization process. Organic templating agents usually play the roles of structure guidance, space filling, and balancing the skeleton charge during the synthesis of molecular sieves, and their content has a great influence on the molecular sieve grain size and crystallinity.[30] As a result, the appropriate concentration of inorganic cations and organic templating agents in the synthetic gel system is essential for the successful synthesis of NaA molecular sieves.

As can be seen from the XRD results in Fig. 1(a) and (b), the diffraction peaks from A1 to A8 all conform to the characteristic peaks of the standard PDF card (PDF#39-0222). This indicates the generation of cubic crystalline NaA molecular sieves. Moreover, it can be observed that changing the organic cation and inorganic templating agent did not affect the surface morphology of the molecular sieves, which indicates that the synthesized NaA molecular sieves have no heterogeneous phases.

To further investigate the influence of inorganic cations (Na_2O) and organic templating (TMAOH) in the synthesis of NaA molecular sieves, the changes in crystallinity for different inorganic cation contents and organic templating agent contents are shown in Fig. 1(b) and 2(b). It is found that the crystallinity of NaA molecular sieves increased obviously when Na_2O/Al_2O_3 increased from 0.15 to 0.3 but decreased when the concentration continued to increase. The crystallinity improved to 89.26% when the organic templating agent concentration was 6. However, a higher concentration did not further improve the crystallinity of NaA. As a result, the crystallinity was optimal at $x = 0.3$ and $y = 6$, respectively.

3.1.2. Morphology analysis. Fig. 3 shows the surface morphology of the NaA molecular sieves. The size of NaA molecular sieves increased significantly with increasing inorganic cation content. This is due to the presence of a low concentration of Na(I) which causes the generation of nano-sized NaA molecular sieves and leads to the formation of a smaller particle size.[31] However, an increase in the content of organic templating agents has the opposite effect. This is because the higher the alkalinity of the organic templating agent, the more silica is soluble, and hence the nucleation rate of the molecular sieves increases.[32] As shown in Fig. 3, no notable change in NaA molecular sieves morphology was observed under FE-SEM. In Fig. 3, the significant decrease in grain size when the content of

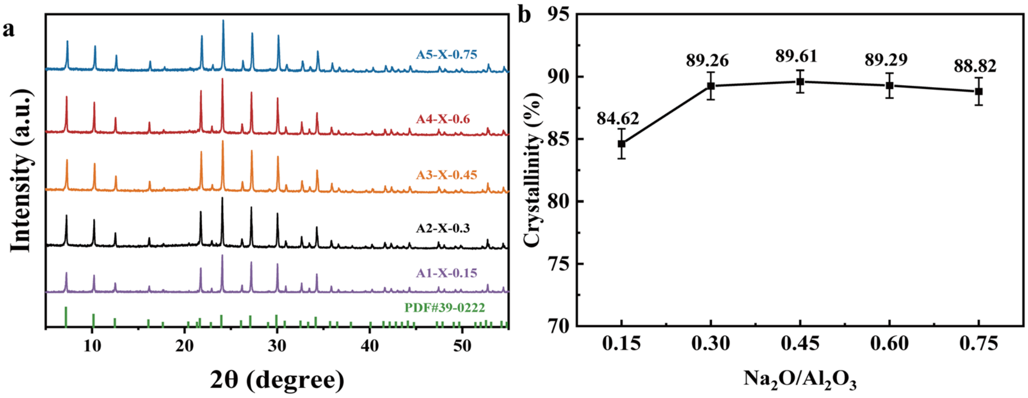

Fig. 1 XRD patterns (a) and crystallinity (b) for NaA molecular sieves with different inorganic cation contents (A1–A5).

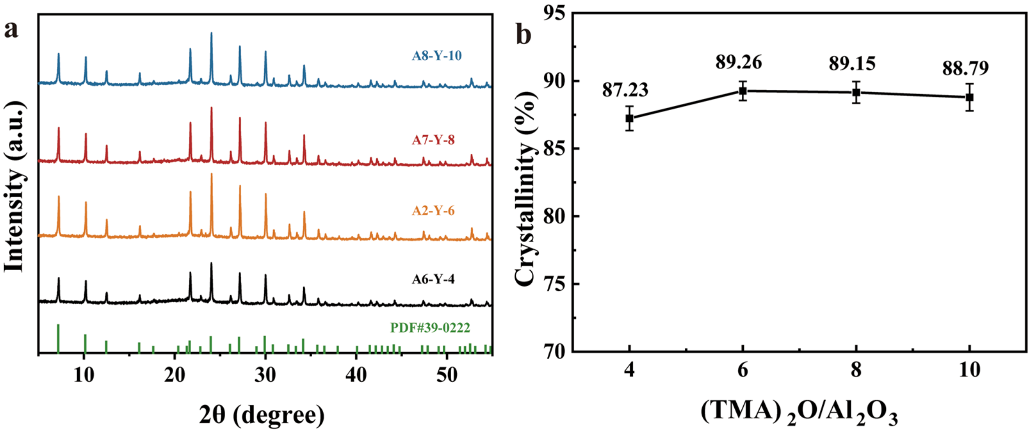

Fig. 2 XRD patterns (a) and crystallinity (b) for NaA molecular sieves with different organic templating agent contents (A6–A8).

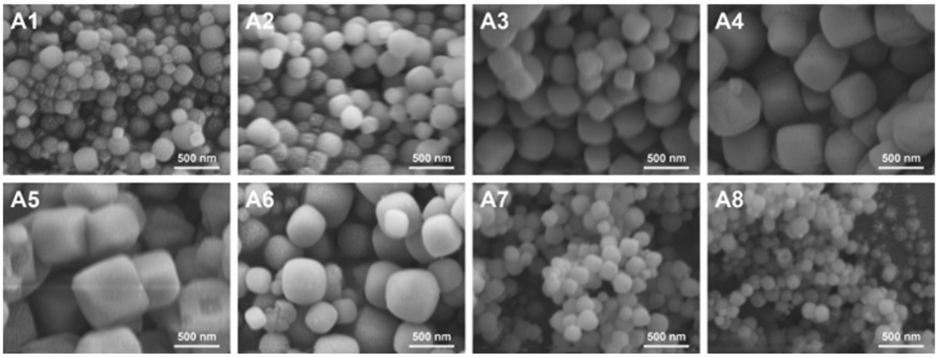

Fig. 3 SEM images of A1–A8.

TMAOH increased from y = 4 (A6) to y = 6 (A2) is due to the higher alkalinity of the organic templating agent increasing the silica solubility, hence increasing the nucleation rate of the molecular sieves. Continuing to increase the templating agent content to y = 8 (A7) and y = 10 (A8), the reduction in grain size was very limited and severe agglomeration occurred, which was probably due to the increased alkalinity and the rise in electrolyte concentration, which caused the condensation of sol–gel particles and other reactions,[32] resulting in the formation of aggregates. Although the individual grain sizes of these aggregates were relatively smaller, some of the products were unable to exhibit the performance of small-sized grains for further use in related applications.

3.1.3. Effect of synthesis parameters on adsorption performance. Fig. 4 shows the effect of cation free concentration on grain size and adsorption characteristics. In Fig. 4(a), the

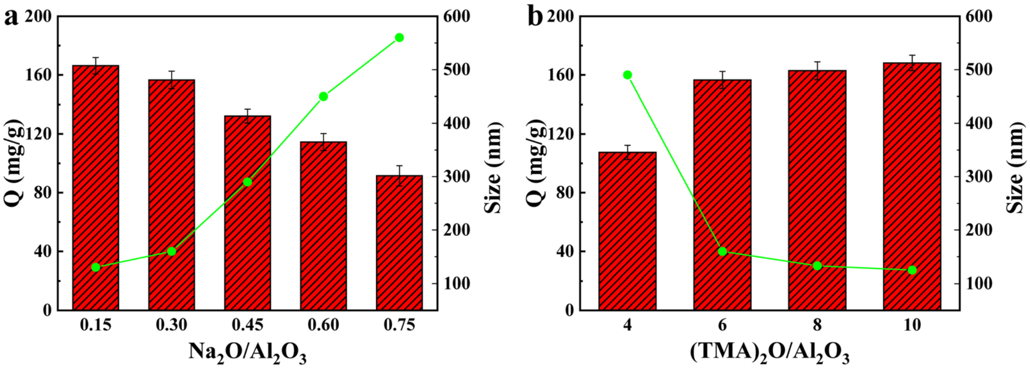

Fig. 4 Adsorption capacity of Cu(II) by NaA molecular sieves with different anodic cation contents (a) and different organic templating agent contents (b).

adsorption capacity decreased with increasing grain size and decreased to 91.5 mg g^{-1} when the grain size reached 560 nm, thus $x = 0.3$ was the optimum content of Na_2O. However, the organic templating agent had a different effect on the amount of adsorption, as shown in Fig. 4(b). With the increase of organic templating agent, the molecular size increased and therefore the adsorption capacity decreases, leading to a decrease in the adsorption capacity. This trend mainly occurs because Na(I) can attract AlO_4^- and SiO_2^- to form large gel particles, increasing the size of anionic cation content.[29] The stronger alkalinity of the templating agent increased the solubility of silica, raising the nucleation rate of the molecular sieve and decreasing the size of TMAOH NaA molecular sieve particles. Smaller molecular sieve sizes enhanced the adsorption performance. As the particle size of the NaA molecular sieve decreased, the amount of adsorption increased. This is probably because the surface area increases with decreasing particle size.[33]

Therefore, combining the results of crystallinity analysis, SEM, XRD and adsorption capacity, we determine that $X = 0.3$, $Y = 6$ is the optimum content of anionic cation and organic templating agent for the synthesis of molecular sieves. Therefore, A2 was used for all subsequent experiments.

3.2. Effects of different parameters on Cu(II) and Pb(II) adsorption

3.2.1. Effect of pH. pH is an important factor in the adsorption process of heavy metal ions. It may affect the morphology of heavy metal ions through corrosion and thus the co-precipitation process.[34] Fig. 5 shows the influence of pH 1–7 on the adsorption capacity of Pb(II) and Cu(II). The adsorption properties increase dramatically as the pH value increases from 1 to 4, and that of Pb(II) and Cu(II) were negligible at pH = 1–2, mostly due to proton exclusion.[35] The adsorption capacity of both Pb(II) and Cu(II) reached a maximum at pH = 5, with maximum values of 230 mg g^{-1} for Cu(II) and 600 mg g^{-1} for Pb(II). Increasing the pH to 7, the adsorption capacity of both heavy metal ions decreased to some extent. The reason is that the excess H^+ would produce competitive adsorption.[11] The skeleton of the molecular sieve is destroyed under acidic conditions.[36] When the pH is too high, OH^- ions increased, and the heavy metal ions were prone to precipitation,[35] which would hinder the adsorption from taking place.[11,20,37] And as adsorption proceeds, the surface of the molecular sieve may be clogged with precipitates. Therefore, pH = 5 was the optimum pH for the adsorption capacity of Cu(II) and Pb(II) by the NaA molecular sieve.

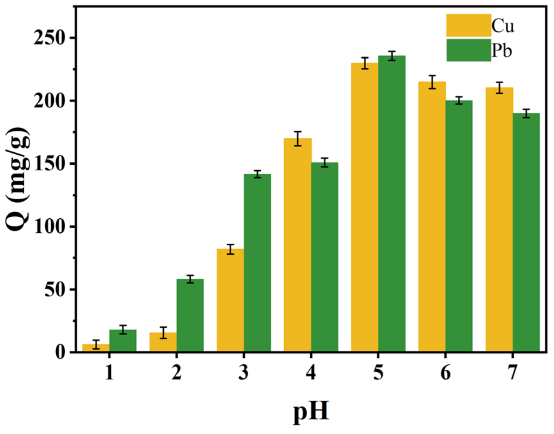

Fig. 5 Adsorption performance for Cu(II) and Pb(II) on NaA molecular sieves at different pH.

3.2.2. Effect of contact time and initial Pb(II) and Cu(II) concentration. The adsorption time analysis and results are presented in Fig. 6. It can be seen that the trend of adsorption of Cu(II) and Pb(II) with different initial concentrations was basically the same. The ability of the NaA molecular sieve to adsorb Cu(II) and Pb(II) increased rapidly initially, and then gradually stabilized. The relationship between the adsorption amount of Pb(II) on the NaA molecular sieve and the time change under different adsorbent concentrations is shown in Fig. 6(a). When the initial concentration of adsorbent was 25 mg L^{-1}, the shortest time to reach the adsorption equilibrium was only 20 min because the adsorption sites were much larger than the required sites for the adsorbent. And the upper adsorption limit of 250 mg g^{-1} was reached. With increasing initial adsorbent concentration, the adsorption reached 450 mg g^{-1} at 50 mg L^{-1}, nearly doubling the adsorption compared to 25 mg L^{-1}. Additionally, the adsorption at 50 mg L^{-1} increased with the initial concentration of adsorbent. The adsorption capacity the equilibrium value reached 540 mg g^{-1} and 600 mg g^{-1} when the concentration of Cu(II) continued to increase at 75 mg L^{-1} and 100 mg L^{-1} respectively. The increase in adsorption amounts also slowed down, which indicated that the adsorption was insufficient to limit the adsorption process. As shown in Fig. 6(b), the amount of Cu(II) adsorption by NaA molecular sieves increased as the initial adsorbent concentration increased, but the magnitude of the increase gradually decreased. The initial adsorbent concentrations of 25 mg L^{-1}, 50 mg L^{-1}, 75 mg L^{-1}, and 100 mg L^{-1} resulted in adsorption amounts of 95 mg g^{-1}, 153 mg g^{-1}, 193 mg g^{-1}, and 230 mg g^{-1}, respectively.

The possible reason for this trend is that the amount of NaA molecular sieves added to the adsorption process was not enough.[17] At the early stage of adsorption, there were sufficient adsorption sites on the NaA molecular sieves, so the growth of adsorption capacity was relatively large. Then the growth of the adsorption amount was limited, which was most likely caused by heavy metal ion saturation of the adsorbent surfaces, followed by adsorption and desorption processes that occur following saturation.[18,38] All adsorption experiments reached equilibrium within 90 min under different initial Cu(II) and Pb(II) concentrations.

3.2.3. Effect of temperature. Fig. 7 provides the adsorption performance of heavy metal ions by NaA molecular sieves at different temperatures. As can be viewed from Fig. 7, the Pb(II) and Cu(II) adsorption also increases gradually when the temperature increases from 25 °C to 55 °C. The reason for this phenomenon is that as the temperature increased, the disorder in the solution increased, which made Cu(II) more easily

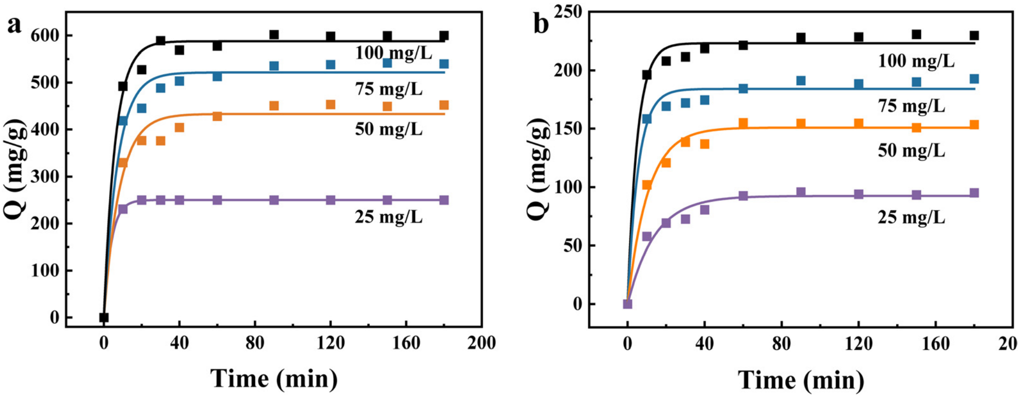

Fig. 6 Adsorption performance of Pb(II) on NaA molecular sieves with different initial adsorbent concentrations (a); adsorption performance of Cu(II) on NaA molecular sieves with different initial adsorbent concentrations (b).

captured by the pores on the NaA molecular sieves. In addition, the effect of temperature on adsorption depends on whether the adsorption is an exothermic or an adsorptive process; for an adsorptive process, an increase in temperature increases the rate of diffusion of ions to the adsorption sites of the adsorbent,[39–41] which facilitates the adsorption process and thus increases the amount of adsorption.

The adsorption amounts of Cu(II) and Pb(II) reached 230 mg g^{-1} and 600 mg g^{-1}, respectively, at an initial adsorbent concentration of 100 mg L^{-1}, an adsorption temperature of 25 °C, and pH = 5. Table S8 (ESI†) compares the adsorption amounts of NaA molecular sieves with those of the other adsorbents, and the adsorption amounts of NaA molecular sieves were more impressive.

3.3. Adsorption isotherms

It is well known that Freundlich and Langmuir isotherms are the most commonly used to define the adsorption of components in solution.[42,43] They are calculated as follows:

$$\ln q_\mathrm{e} = \ln K_\mathrm{F} + \frac{1}{n}\ln C_\mathrm{e} \tag{2}$$

$$\frac{C_\mathrm{e}}{q_\mathrm{e}} = \frac{C_\mathrm{e}}{q_\mathrm{max}} + \frac{1}{K_\mathrm{L}q_\mathrm{max}} \tag{3}$$

where q_e (mg g^{-1}), K_L, K_F and q_max (mg g^{-1}) represent the adsorbed amount at the adsorption equilibrium, the Langmuir rate constant, the Freundlich rate constant, and the theoretically achievable adsorption amount, respectively. C_e (mg L^{-1}) represents the concentration of heavy metal ion in the solution at the equilibrium of adsorption. Plotting the equilibrium concentration C_e as the independent variable with respect to q_e, the theoretical limiting adsorption quantity q_max and rate constant K_L can be obtained from the intercept and slope.

The equilibrium adsorption data for Pb(II) and Cu(II) at different temperatures were fitted to the isotherm equation. As shown in Fig. 8, the experimental data for both metal ions are consistent with the Langmuir isothermal model. Generally, the value of R^2 determines the type of isotherm;[44] the closer the value of R^2 is to 1, the better the fit is. In Tables S2 and S3 (ESI†), the Langmuir isothermal showed better fitting. This indicates that the adsorption process of Cu(II) and Pb(II) on the surface of NaA molecular sieves is not a multilayer inhomogeneous adsorption.[27,45,46]

3.4. Adsorption kinetics

Two different kinetic models were used to simulate the kinetic behavior of Pb(II) and Cu(II) adsorption on NaA molecular sieves. The linear equations of the pseudo-first-order (PFO) and pseudo-second-order (PSO) kinetic models are shown in the following equations.[18,47]

Eqn (4) is the pseudo-first-order (PFO) kinetic model

$$\ln(q_\mathrm{e} - q_\mathrm{t}) = \ln q_\mathrm{e} - K_1 t \tag{4}$$

Eqn (5) is the pseudo-second-order (PSO) kinetic model

$$\frac{t}{q_\mathrm{t}} = \frac{1}{K_2 {q_\mathrm{e}}^2} + \frac{t}{q_\mathrm{e}} \tag{5}$$

where q_e (mg g^{-1}) is the adsorbed amount at adsorption equilibrium, q_t (mg g^{-1}) is the adsorbed amount at an

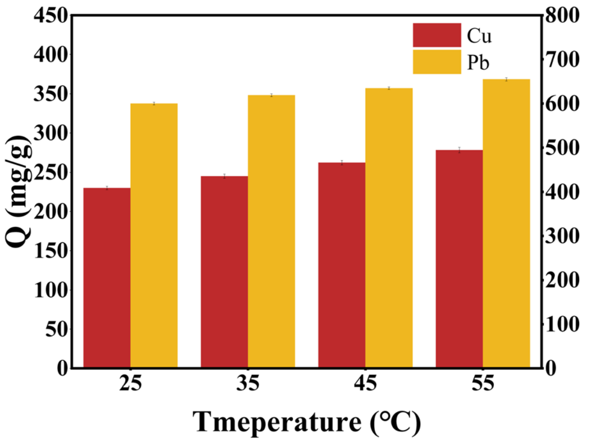

Fig. 7 Adsorption properties of Pb(II) and Cu(II) on NaA molecular sieves at different temperatures.

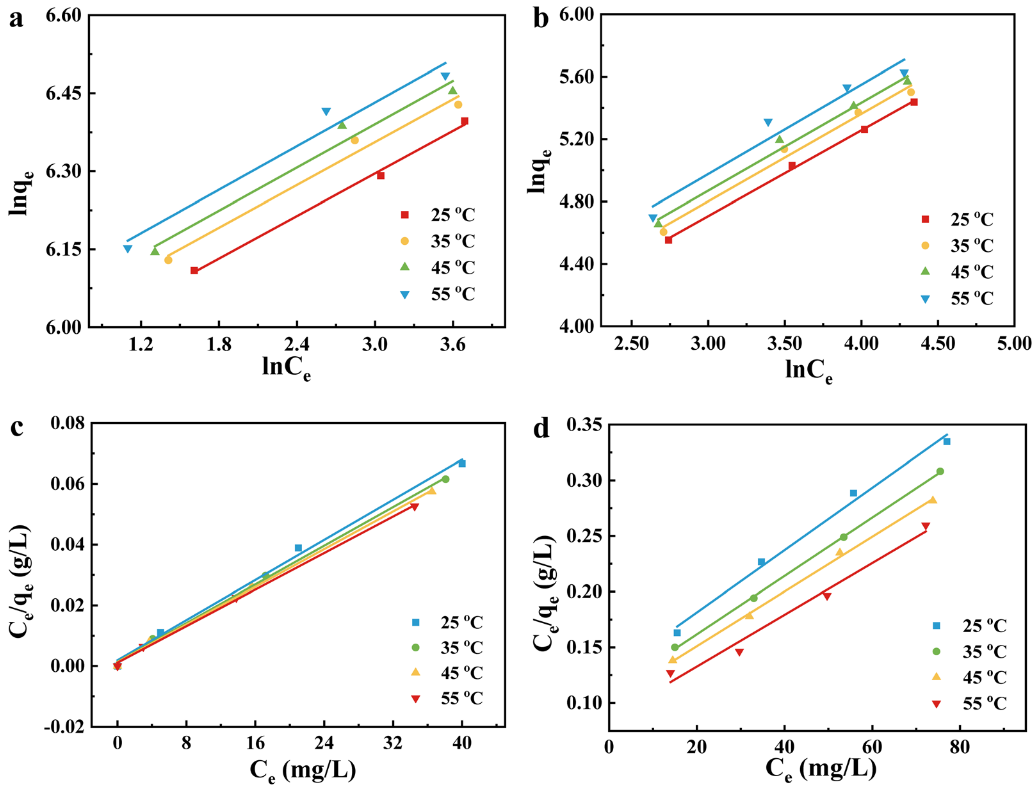

Fig. 8 Freundlich adsorption isotherms of heavy metal ions on NaA molecular sieves at different temperatures, the adsorption of Pb(II) (a) and the adsorption of Cu(II) (b). Langmuir adsorption isotherms of heavy metal ions on NaA molecular sieves at different temperatures, the adsorption of Pb(II) (c), and the adsorption of Cu(II) (d).

adsorption time of t (min), and K_1 and K_2 represent the rate constants for quasi-primary and quasi-secondary kinetics, respectively.

Fig. 9 shows the fitting of the quasi-primary kinetic model for Cu(II) and Pb(II) and the fitting of the quasi-secondary kinetic model. As shown in Fig. 9(a) and (b), the large difference indicates that the quasi-primary kinetic model cannot accurately represent the adsorption processes of Cu(II) and Pb(II) by NaA molecular sieves. The parameters of the quasi-primary kinetic model and the quasi-secondary kinetic model are shown in Tables S4 and S5 (ESI†), while the majority of the correlation coefficients R^2 for the first kinetic model were below 0.9, and all of the values of R^2 for the second kinetic model were over that threshold. At a starting Cu(II) concentration of 25 mg L^{-1}, the correlation coefficient was just 0.7882. And the closer the correlation coefficient is to 1, the better the fit is represented. Summarizing the results mentioned above, the pseudo-second order model strongly fits the adsorption of two heavy metal ions. The adsorption modeling data of NaA molecular sieves implied that the adsorption of heavy metal ions may be chemisorption.[48,49]

3.5. Thermodynamic study

The effect of temperature on Cu(II) and Pb(II) adsorption by the NaA molecular sieve was studied at different temperatures including 298, 308, 318 and 328 K. The experiment used the following eqn (6)–(10).

$$K = \frac{q_e}{C_e} \quad (6)$$

$$\Delta G = -RT\ln K \quad (7)$$

$$\Delta G = \Delta H - T\Delta S \quad (9)$$

$$\ln K = -\frac{\Delta H}{RT} + \frac{\Delta S}{R} \quad (10)$$

where K, q_e, C_e, R, T, ΔG, ΔH, and ΔS denote the equilibrium constant, concentration of adsorbate on adsorbent (mg g^{-1}), concentration of adsorbate in solution (mg L^{-1}), ideal gas constant (8.314 J mol^{-1} K^{-1}), thermodynamic temperature (K), Gibbs free energy (kJ mol^{-1}), enthalpy change (kJ mol^{-1}), and entropy change (J mol^{-1} K^{-1}).

Fig. 10 is the thermodynamic fitting diagram, and the thermodynamic parameters are shown in Table S6 (ESI†). ΔH was positive for different temperatures and adsorbents, which indicated that the adsorption of Cu(II) and Pb(II) by NaA molecular sieves is a heat-absorbing process,[50] and the increase of temperature was favorable for the adsorption, which also confirmed our previous conclusions. ΔS indicates the degree of disorder in the adsorption system, and $\Delta S > 0$ indicates that the adsorption process proceeds in the direction of increasing disorder. In addition, ΔG was all negative, which indicated that both adsorption processes

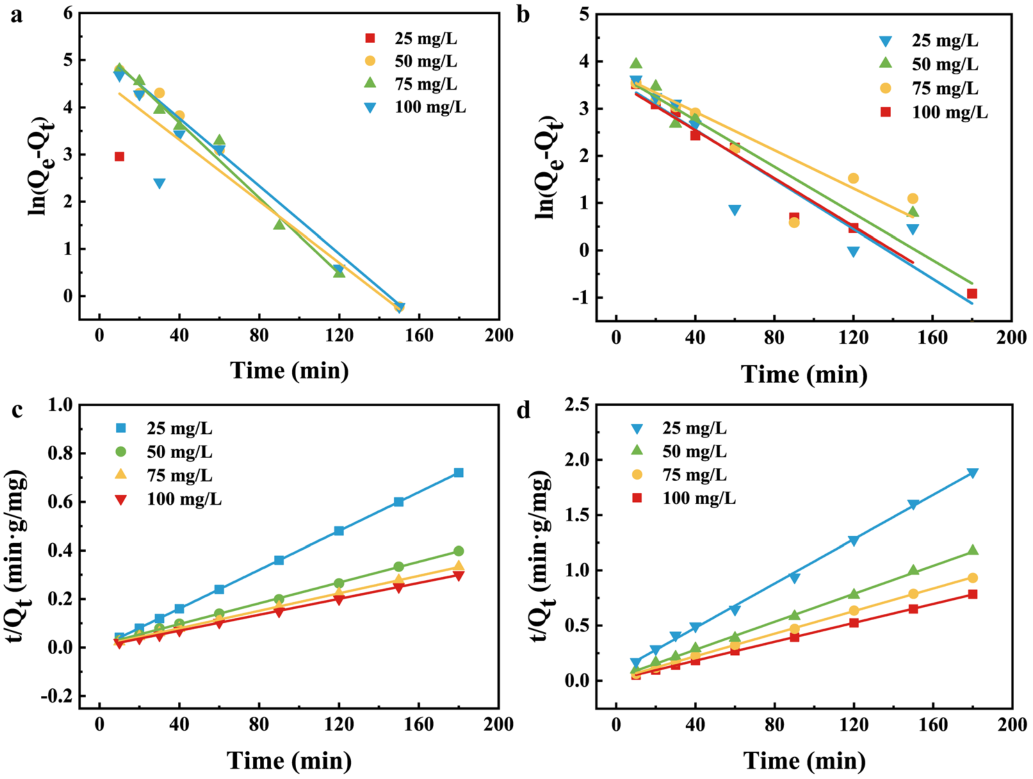

Fig. 9 Quasi-primary kinetic modelling of NaA molecular sieve adsorption at different heavy metal ion concentrations, Pb(II) (a), and Cu(II) (b). Quasi-secondary kinetic modelling of NaA molecular sieve adsorption at different heavy metal ion concentrations, Pb(II) (c), and Cu(II) (d).

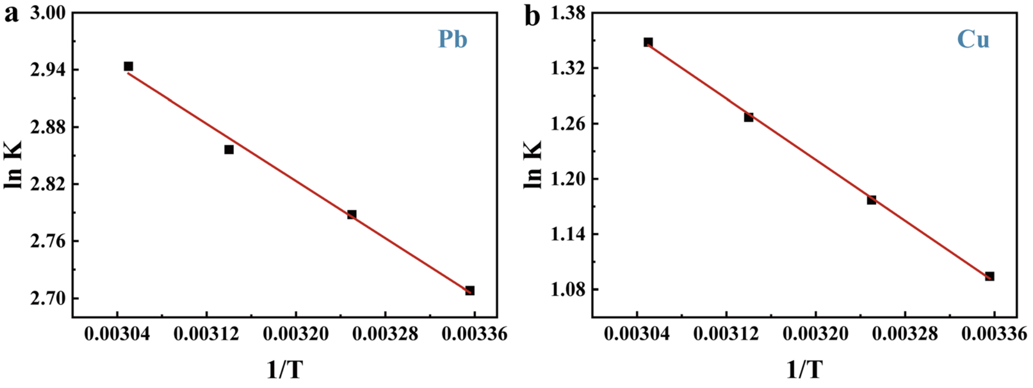

Fig. 10 Thermodynamic fitting of Pb(II) (a) and Cu(II) (b) adsorption on NaA molecular sieves.

were spontaneous,[51,52] and ΔG decreased with increasing temperature, which once again proved that increasing temperature promoted this adsorption process.[53]

3.6. Adsorption mechanism studies

Fig. 11 shows SEM-EDX images of NaA molecular sieves before and after adsorption of heavy metal ions Cu(II) and Pb(II). Before adsorption, elements (O, Al, Si, Na) could be detected on the surface of NaA molecular sieves. After the adsorption of Cu(II) and Pb(II), Cu(II) and Pb(II) could be detected on the surface of the NaA molecular sieve, which proved that adsorption reaction occurred. In addition, the content of Na element almost disappeared after adsorption. This may be due to the ion exchange process of the NaA molecular sieve, where Na(I) was replaced by Cu(II) and Pb(II) and reduced.

XPS analyses were carried out before and after adsorption to further explain the adsorption mechanism. The XPS full spectra of NaA molecular sieves before and after Cu(II) and Pb(II) adsorption are shown in Fig. S1 (ESI†). After adsorption, there was little change in the peaks of O 1s, Si 2p and Al 2p, and the appearance of the peaks of Cu 2p and Pb 4f confirmed the adsorption effect of NaA molecular sieves. The comparison of the full XPS spectra before and after adsorption revealed that the intensity of the peaks of Na 1s almost disappeared after

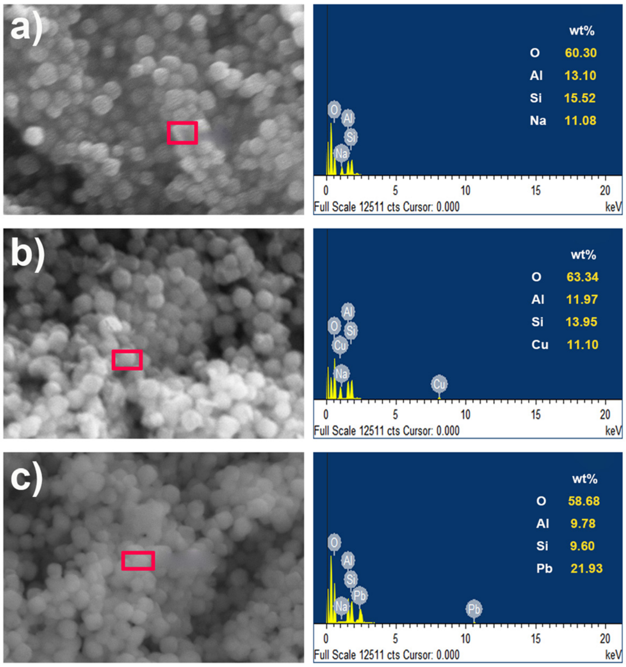

Fig. 11 EDX energy spectra of NaA molecular sieves before adsorption (a), and after adsorption of Cu(II) (b) and Pb(II) (c).

adsorption, implying that Na and Cu(II) and Pb(II) were ion-exchanged. The fine spectra of Cu 2p and Pb 4f of the adsorbed samples are analyzed in Fig. 12(a), where the peaks at 935.6 eV and 955.25 eV correspond to the Cu 2p3/2 and Cu 2p1/2 orbitals, respectively, whereas the peaks at 942.35 eV, 944.65 eV, and 964.8 eV are satellite peaks induced by Cu(II).[54] The peaks at 140.7 eV and 145.6 eV also correspond to Pb 4f5/2 and Pb 4f7/2 orbitals[55] as shown in Fig. 12(b). These results proved that Cu(II) and Pb(II) were successfully adsorbed on NaA molecular sieves. Therefore, we can conclude that the adsorption mechanism of Cu(II) and Pb(II) may be the ion exchange between Na(I) and Cu(II) and Pb(II), and the adsorption mechanism is depicted in Fig. 13.

As shown in Fig. S2 (ESI†), the XRD peak signals became weaker when the Pb(II) and Cu(II) were adsorbed on the NaA molecular sieves, which may be due to the reduced amount of samples taken for testing.[56] However, from the overall view, no new peaks were generated. This indicates that the cubic crystalline shape of the molecular sieves was not destroyed and no new crystalline shape was generated due to adsorption. We carried out Fourier transform infrared analysis of the molecular sieves before and after the adsorption of heavy metal ions, as shown in Fig. S3 (ESI†), and comparing the spectra of NaA, NaA–Pb and NaA–Cu the positions of the absorption peaks were basically the same, which indicated that there was no change in the chemical structure of the NaA molecular sieves after the adsorption of Pb and Cu. As shown in the Fig. S3 (ESI†), the peaks around 459–461 $\mathrm{cm^{-1}}$ and 541–547 $\mathrm{cm^{-1}}$ were the vibration peaks of the NaA molecular sieve skeleton. And the peaks at 967–973 $\mathrm{cm^{-1}}$ were the characteristic absorption peaks of Al–O and Si–O of the NaA molecular sieves.[57–59]

BET tests were conducted on NaA molecular sieves both before and after absorbing heavy metals. The NaA molecular sieves with absorbed Pb(II) were named NaA–Pb, while those with absorbed Cu(II) were labeled NaA–Cu. As shown in Fig. 14(a), the molecular sieves before and after adsorption showed obvious H3-type hysteresis loops,[60] which exhibited the characteristics of mesoporous channels. Fig. 14(b) shows that NaA molecular sieves before and after adsorption of heavy metals exhibited large amounts of mesopores, except for a small number of mesopores before and after the adsorption of heavy metals on NaA molecular sieves. The specific surface area and pore size values of the molecular sieves before and after absorbing heavy metal ions are detailed in Table S9 (ESI†). The specific surface area of NaA decreased from 36.86 $\mathrm{m^2\ g^{-1}}$ to 21.86 $\mathrm{m^2\ g^{-1}}$ and 31.66 $\mathrm{m^2\ g^{-1}}$ after absorbing Pb(II) and Cu(II), respectively. The average pore size of NaA was 21.91 nm, while the pore sizes of NaA–Pb and NaA–Cu were 26.79 nm and 25.41 nm, respectively. The decrease in specific surface area and increase in pore size after absorption can be attributed to the exchange of two $\mathrm{Na^+}$ ions with one heavy metal ion, leading

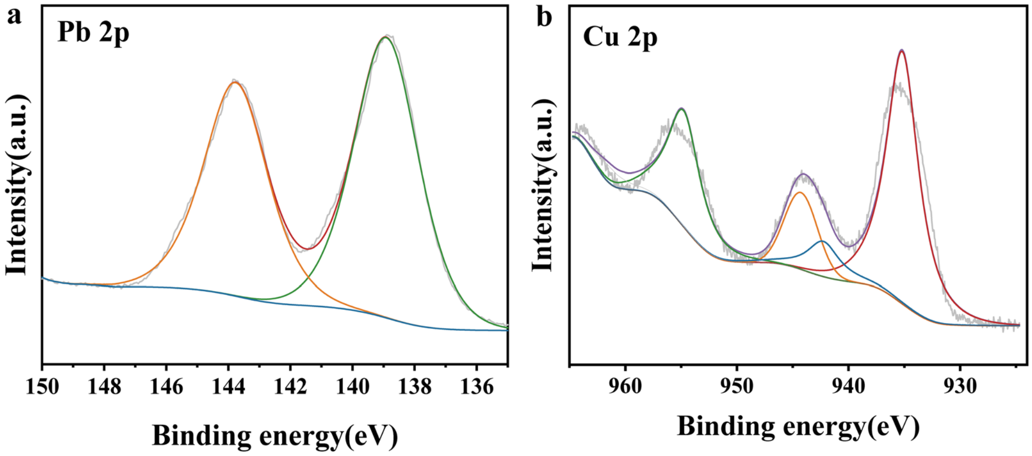

Fig. 12 XPS spectra of Cu(II) (a) and Pb(II) (b) adsorbed on NaA molecular sieves.

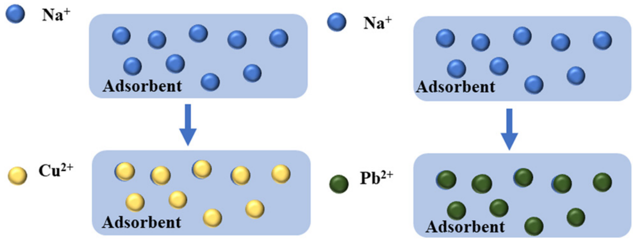

Fig. 13 NaA molecular sieve adsorption mechanism diagram.

to larger pore sizes.[61] And the exchanged heavy metal may bind the hydroxyl group and produce precipitation, covering in the pore channel of the molecular sieve, resulting in a smaller specific surface.[62,63] And the specific surface area of NaA–Pb is much reduced compared with that of NaA–Cu, mainly because the NaA molecular sieve adsorbs more Pb(II), so more heavy metal ions accumulate in the molecular sieve pores.

3.7. NaA molecular sieves regeneration-cycle adsorption

Reusability is a crucial property of adsorbents. In this study, we explored the ability of NaA molecular sieves to repeatedly adsorb the heavy metal ions Cu and Pb. As illustrated in Fig. 15, over four cycles of desorption and re-sorption the molecular sieve's adsorption capacity for heavy metals decreased with each cycle. Before desorption, the adsorption of Pb(II) and Cu(II) by the molecular sieve was 230 mg g^{-1} and 600 mg g^{-1}, respectively. By the fourth cycle, Cu(II) adsorption decreased to 403 mg g^{-1} and Pb(II) adsorption to 121 mg g^{-1}. Despite the gradual decline, the molecular sieve retained a significant adsorption capacity after four cycles, demonstrating its strong reusability.

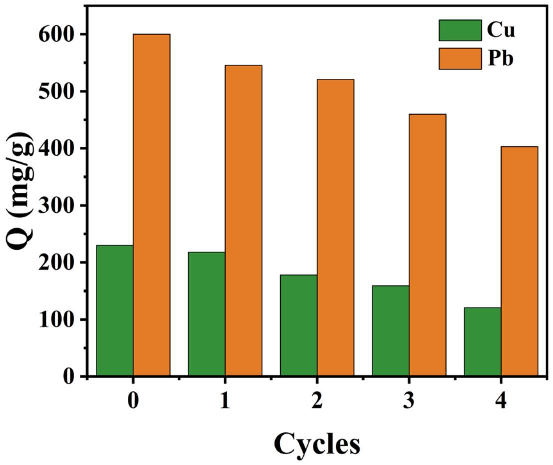

Fig. 15 The amount of Cu(II) and Pb(II) desorption and re-sorption cycle experiments on NaA molecular sieves.

4. Conclusion

In this study, we significantly reduced the size of NaA molecular sieves and enhanced the adsorption capacity for heavy metal ions Pb and Cu by adjusting the ratio of metal cations and inorganic templating agents. The results revealed that by adjusting the ingredient ratio to $Al_2O_3 : SiO_2 : Na_2O : (TMA)_2O : H_2O = 1 : 2 : 0.3 : 6 : 350$, the particle size of the molecular sieves was 10 times smaller than conventional commercial ones, but still with higher crystallinity. We examined the optimal adsorption pH, temperature, and equilibrium time through heavy metal ion adsorption experiments. The adsorption efficiency of Cu(II) and Pb(II) reached 230 mg g^{-1} and 600 mg g^{-1}, respectively, at an initial adsorbent concentration of 100 mg L^{-1}, an adsorption temperature of 25 °C, and pH = 5. The Langmuir isothermal model accurately characterizes the monolayer adsorption process of NaA molecular sieves on Cu(II) and Pb(II), while the thermodynamic analysis indicates $\Delta G < 0$, suggesting a spontaneous heat absorption process during adsorption. In addition, the NaA molecular sieve shows strong structural and performance stability after being used four times. Therefore, this NaA molecular sieve presents as an efficient and reusable nanoscale molecular sieve with promising industrial potential.

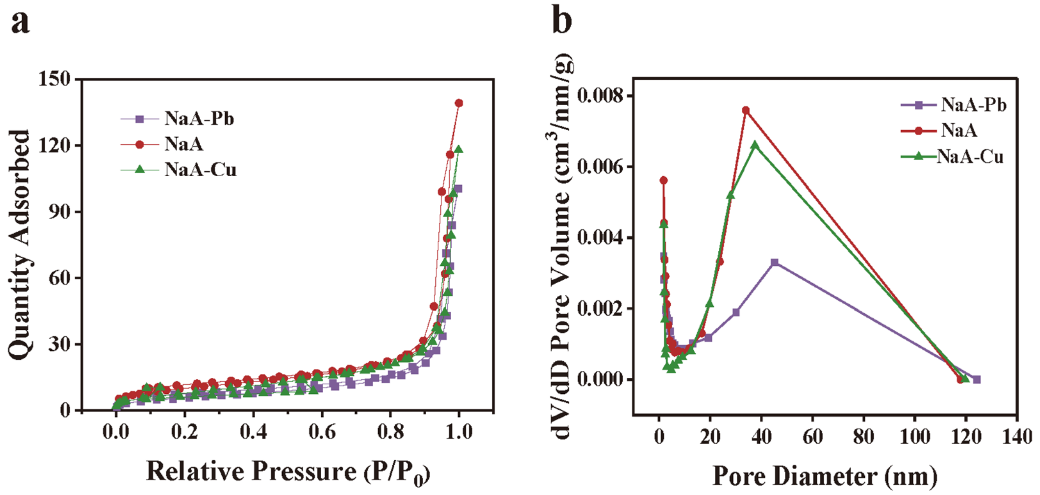

Fig. 14 N_2 adsorption and desorption isotherms of NaA molecular sieves before and after adsorption of heavy metal ions (a) and pore size distribution (b).

Author contributions

K. T. and L. W. C. conceived the study and designed the experiments. K. T. and W. L. C. performed the experiments. W. L. C. wrote the article together. W. G. L, Z. C. and Y. B. H. revised the article. All authors approved the article for publication.

Conflicts of interest

There are no conflicts to declare.

Acknowledgements

This work was supported by Suntar Membrane Technology (Xiamen) Co., Ltd, Xiamen.

References

1 X. J. Hu, Y. G. Liu, H. Wang, A. W. Chen, G. M. Zeng, S. M. Liu, Y. M. Guo, X. Hu, T. T. Li, Y. Q. Wang, L. Zhou and S. H. Liu, *Sep. Purif. Technol.*, 2013, **108**, 189–195.
2 M. Cartró-Sabaté, P. Mayor, M. Orta-Martínez and A. Rosell-Melé, *Nat. Sustainability*, 2019, **2**, 702–709.
3 H.-Y. Niu, X. Li and J. Li, *New J. Chem.*, 2022, **46**, 5234–5245.
4 C. Jin, G. Teng, Y. Gu, H. Cheng, S. Fu, C. Zhang and W. Ma, *New J. Chem.*, 2019, **43**, 5879–5889.
5 E. Panousi, D. Mamais, C. Noutsopoulos, K. Antoniou, K. Koutoula, S. Mastrantoni, C. Koutsogiannis and A. Gkioni, *J. Chem. Technol. Biotechnol.*, 2016, **91**, 1681–1687.
6 J. Wang and X. Guo, *Crit. Rev. Environ. Sci. Technol.*, 2023, **53**, 1837–1865.
7 M. Z. Momcilovic, M. S. Randelovic, M. M. Purenovic, J. S. Dordevic, A. Onjia and B. Matovic, *Sep. Purif. Technol.*, 2016, **163**, 72–78.
8 A. Mojiri, J. L. Zhou, B. Robinson, A. Ohashi, N. Ozaki, T. Kindaichi, H. Farraji and M. Vakili, *Chemosphere*, 2020, 253.
9 L. Shi, B. Duan, Z. Zhu, C. Sun, J. Zhou and A. Walsh, *Ultrason. Sonochem.*, 2020, 64.
10 X. Yin, Z. J. Zhang, H. Y. Ma, S. Venkateswaran and B. S. Hsiao, *Sep. Purif. Technol.*, 2020, 242.
11 G. Li, X. Qi, N. Yang, X. Duan and A. Zhang, *Chemosphere*, 2022, 301.
12 R. Wang, L. Deng, X. Fan, K. Li, H. Lu and W. Li, *Int. J. Biol. Macromol.*, 2021, **189**, 607–617.
13 B. Y. Wang, J. M. Lan, C. M. Bo, B. L. Gong and J. J. Ou, *RSC Adv.*, 2023, **13**, 4275–4302.
14 H. Y. Ren, H. Y. Shen and Y. Z. Liu, *J. CO2 Util.*, 2022, 58.
15 Z. Y. Yang, D. C. Wang, Z. Y. Meng and Y. Y. Li, *Sep. Purif. Technol.*, 2019, **218**, 130–137.
16 A. B. Saralegui, V. Willson, N. Caracciolo, M. N. Piol and S. P. Boeykens, *J. Environ. Manage.*, 2021, 289.
17 J. Shahrivar and M. Gharabaghi, *Adv. Powder Technol.*, 2020, **31**, 4648–4656.
18 K. Wang, L. Yang, H. Li and F. Zhang, *ACS Appl. Mater. Interfaces*, 2019, **11**, 21815–21821.
19 G. Li, B. Wang, Q. Sun, W. Q. Xu and Y. Han, *Microporous Mesoporous Mater.*, 2017, **252**, 105–115.
20 Z. Liang, Q. Gao, Z. Wu and H. Gao, *Environ. Sci. Pollut. Res.*, 2022, **29**, 84651–84660.
21 C. Wang, Q. Sun, L. Zhang, T. Su and Y. Yang, *J. Environ. Chem. Eng.*, 2022, 10.
22 V. Valtchev and L. Tosheva, *Chem. Rev.*, 2013, **113**, 6734–6760.
23 K. Zhu, J. Sun, J. Liu, L. Wang, H. Wan, J. Hu, Y. Wang, C. H. F. Peden and Z. Nie, *ACS Catal.*, 2011, **1**, 682–690.
24 G.-T. Vuong, V.-T. Hoang, D.-T. Nguyen and T.-O. Do, *Appl. Catal., A*, 2010, **382**, 231–239.
25 Y. Ren, F. Wu, G. Qu, N. Ren, P. Ning, X. Chen, M. He, Y. Yang, Z. Wang and Y. Hu, *J. Mater. Res. Technol.*, 2023, **23**, 3023–3034.
26 Y. Chen, A. Armutlulu, W. Sun, W. Jiang, X. Jiang, B. Lai and R. Xie, *Sci. Total Environ.*, 2020, 714.
27 J. Gao, Q. Lin, T. Yang, Y. C. Bao and J. Liu, *Chemosphere*, 2023, **341**, 139741.
28 A. S. Huang and W. S. Yang, *Sep. Purif. Technol.*, 2008, **61**, 175–181.
29 C. S. Cundy and P. A. Cox, *Chem. Rev.*, 2003, **103**, 663–701.
30 S. Mintova, J.-P. Gilson and V. Valtchev, *Nanoscale*, 2013, 5.
31 M. T. Melchior, D. E. W. Vaughan and C. F. Pictroski, *J. Phys. Chem.*, 1995, **99**, 6128–6144.
32 S. Mintova, N. H. Olson, V. Valtchev and T. Bein, *Science*, 1999, **283**, 958–960.
33 E. I. Ugwu, O. Tursunov, D. Kodirov, L. M. Shaker, A. A. Al-Amiery, I. Yangibaeva and F. Shavkarov, *IOP Conf. Ser.: Earth Environ. Sci.*, 2020, **614**, 012166.
34 Z. Yang, J. Ma, F. Liu, H. Zhang, X. Ma and D. He, *J. Colloid Interface Sci.*, 2022, **608**, 864–872.
35 C. Feng, M. Huang and C.-P. Huang, *Chem. Eng. J.*, 2023, 451.
36 R. Wang, L. Deng, X. Fan, K. Li, H. Lu and W. Li, *Int. J. Biol. Macromol.*, 2021, **189**, 607–617.
37 N. Esfandiar, R. Suri and E. R. McKenzie, *J. Hazard. Mater.*, 2022, 423.
38 M. E. Argun, S. Dursun, C. Ozdemir and M. Karatas, *J. Hazard. Mater.*, 2007, **141**, 77–85.
39 X. Liu and R. Wang, *J. Hazard. Mater.*, 2017, **326**, 157–164.
40 B. Qiu, Q. Shao, J. Shi, C. Yang and H. Chu, *Sep. Purif. Technol.*, 2022, **300**, 121925.
41 N. K. Soliman and A. F. Moustafa, *J. Mater. Res. Technol.*, 2020, **9**, 10235–10253.
42 Z. Yang, D. Wang, Z. Meng and Y. Li, *Sep. Purif. Technol.*, 2019, **218**, 130–137.
43 D.-H. Vu, H.-B. Bui, X.-N. Bui, D. An-Nguyen, Q.-T. Le, N.-H. Do and H. Nguyen, *Int. J. Environ. Anal. Chem.*, 2019, **100**, 1226–1244.
44 H. Xue, X. Gao, M. K. Seliem, M. Mobarak, R. Dong, X. Wang, K. Fu, Q. Li and Z. Li, *Chem. Eng. J.*, 2023, 451.
45 L. Li, X. Liu, T. Duan, F. Xu, A. Abdulkhani and X. Zhang, *Bioresour. Technol.*, 2023, 376.

46 H. Luo, W. W. Law, Y. Wu, W. Zhu and E.-H. Yang, *Microporous Mesoporous Mater.*, 2018, **272**, 8–15.
47 D. Huang, Y. Liu, Y. Liu, D. Di, H. Wang and W. Yang, *New J. Chem.*, 2019, **43**, 7243–7250.
48 K. Li, J. Hu, Z. Liu, L. Chen and Y. Dong, *J. Radioanal. Nucl. Chem.*, 2012, **295**, 2125–2133.
49 J. R. Koduru, L. P. Lingamdinne, S. K. Kailasa, T. Thenepalli, Y.-Y. Chang and J.-K. Yang, in *Rare-Earth Metal Recovery for Green Technologies: Methods and Applications*, ed. R. K. Jyothi, Springer International Publishing, Cham, 2020, pp. 87–109.
50 N. A. Alamrani, H. A. Al-Aoh, M. M. H. Aljohani, S. A. Bani-Atta, M. Sobhi, M. Syed Khalid, A. A. A. Darwish, A. A. Keshk, M. A. A. Abdelfattah and M. N. Nadagouda, *J. Chem.*, 2021, 1–10.
51 H. Al-Johani and M. A. Salam, *J. Colloid Interface Sci.*, 2011, **360**, 760–767.
52 T. Adhikari and M. V. Singh, *Geoderma*, 2003, **114**, 81–92.
53 X.-J. Hu, Y.-G. Liu, H. Wang, A.-W. Chen, G.-M. Zeng, S.-M. Liu, Y.-M. Guo, X. Hu, T.-T. Li, Y.-Q. Wang, L. Zhou and S.-H. Liu, *Sep. Purif. Technol.*, 2013, **108**, 189–195.
54 X. W. Du, S. P. Luo, H. Y. Du, M. Tang, X. D. Huang and P. K. Shen, *J. Mater. Chem. A*, 2016, **4**, 1579–1585.
55 D. Roy, S. Neogi and S. De, *J. Hazard. Mater.*, 2021, 403.
56 J. Zhang, C. Tian, Y. Xu, J. Chen, L. Xiao, G. Wu and F. Jin, *Sep. Purif. Technol.*, 2023, 305.
57 Q. Du, H. Xu, Z. Yu, B. Liu, Q. Peng, D. Li, T. Ben and H. Yu, *J. Phys.: Conf. Ser.*, 2022, **2168**, 012026.
58 W. Yuan, H. Chen, R. Chang and L. Li, *Desalination*, 2011, **273**, 343–351.
59 K. Wang, F. Wang, F. Chen, X. Cui, Y. Wei, L. Shao and M. Yu, *ACS Sustainable Chem. Eng.*, 2019, **7**, 2459–2470.
60 P. A. Monson, *Microporous Mesoporous Mater.*, 2012, **160**, 47–66.
61 L. Lv, G. Tsoi and X. S. Zhao, *Ind. Eng. Chem. Res.*, 2004, **43**, 7900–7906.
62 P. Maneechakr and S. Mongkollertlop, *J. Environ. Chem. Eng.*, 2020, 8.
63 S. M. Hosseini, H. Alibakhshi, E. Jashni, F. Parvizian, J. N. Shen, M. Taheri, M. Ebrahimi and N. Rafiei, *J. Hazard. Mater.*, 2020, **381**, 120884.